

### **PAPER • OPEN ACCESS**

# C-band InAs/InP quantum dots: alternative growth versus indium-flush for self-assembled growth

To cite this article: Jiajing Yuan et al 2025 Semicond. Sci. Technol. 40 105013

View the article online for updates and enhancements.

# You may also like

- Effect of annealing temperature on the optoelectronic properties of quinary amorphous oxide semiconductor IGZTO thin films
- Zhiyi Li, Liang Fang, Hongyu Wu et al.
- Simulation and optimization of perovskite solar cells with multifunctional polymer interlayers at the perovskite/HTM interface Diego Alberto Liña-Martínez, Liliana Hechavarría-Difur, Joel Pantoja-Enríquez et al.
- Investigation of defect evolution in 4H-SiC epitaxial layers via scratch-etching method Jingyi Jiao, Siqi Zhao, Yunkai Li et al.



Semicond. Sci. Technol. 40 (2025) 105013 (9pp)

https://doi.org/10.1088/1361-6641/ae10d5

# C-band InAs/InP quantum dots: alternative growth versus indium-flush for self-assembled growth

Jiajing Yuan<sup>1</sup>, Hui Jia<sup>1,\*</sup>, Calum Dear<sup>1</sup>, Huiwen Deng<sup>1,\*</sup>, Mateus G Masteghin<sup>2</sup>, Khalil El Hajraoui<sup>3,4</sup>, Jun Li<sup>1</sup>, Kongming Liu<sup>1</sup>, Mengxun Bai<sup>1</sup>, Jakob B Wagner<sup>2</sup>, Quentin M Ramasse<sup>3,5</sup>, Mingchu Tang<sup>1</sup>, Alwyn Seeds<sup>1</sup> and Huiyun Liu<sup>1</sup>

E-mail: hui.jia@ucl.ac.uk and huiwen.deng@ucl.ac.uk

Received 8 July 2025, revised 8 September 2025 Accepted for publication 8 October 2025 Published 27 October 2025



#### Abstract

1550 nm InAs/InP quantum dot (QD) lasers are critical for C-band optical communication. To realise narrow photo-luminescence linewidth emission in this wavelength range, the indium flush (IF) technique for self-assembled QDs and the alternative growth (AG) technique have been developed, enabling wavelength tuning and control of dot uniformity. This work investigates the stacking effect on nanostructures grown by these two methods by comparing five-stacked AG and IF nanostructures with identical spacer thickness. Structural and optical characterisations were performed using scanning transmission electron microscopy, atomic force microscopy, and photoluminescence measurements. The IF approach produces truncated, height-controlled QDs with reduced strain accumulation across stacked layers. In contrast, AG samples display quantum well-like morphology with sharp interfaces and no observable dislocations, but fail to consistently produce distinct QD nanostructures. These results suggest that IF provides a more reliable optimisation strategy for achieving C-band QDs within the framework of self-assembled growth, whereas AG requires further optimisation for use in InP-based systems.

Keywords: InAs/InP, quantum dots, C-band communication, molecular beam epitaxy

Original content from this work may be used under the terms of the Creative Commons Attribution 4.0 licence. Any further distribution of this work must maintain attribution to the author(s) and the title of the work, journal citation and DOI.

<sup>&</sup>lt;sup>1</sup> Department of Electronic and Electrical Engineering, University College London, London WC1E 7JE, United Kingdom

<sup>&</sup>lt;sup>2</sup> DTU Nanolab, Technical University of Denmark, Fysikvej, Kongens Lyngby 2800, Denmark

<sup>&</sup>lt;sup>3</sup> SuperSTEM, SciTech Daresbury Science and Innovation Campus, Block J, Keckwick Lane, Daresbury WA4 4AD, United Kingdom

<sup>&</sup>lt;sup>4</sup> York NanoCentre & Department of Physics, University of York, York YO10 5DD, United Kingdom

<sup>&</sup>lt;sup>5</sup> School of Chemical and Process Engineering and School of Physics and Technology, University of Leeds, Leeds LS29JT, United Kingdom

<sup>\*</sup> Authors to whom any correspondence should be addressed.

#### 1. Introduction

High-performance lasers operating in the C-band wavelengths are increasingly in demand as light sources for optical communication, driven by the rapid increase in data traffic and the steep expansion of artificial intelligence-related applications [1–3]. To meet these stringent requirements, self-assembled quantum dot (QD) lasers have attracted considerable attention due to their atom-like discrete energy states [4–6]. The delta-function-like density of states and the large energy separation between the ground state and the first excited state enable low threshold current density, temperature insensitivity, and ultra-fast gain recovery [5, 7–9]. To achieve emission at Cband wavelengths, InP-based InAs QDs are widely employed. However, the anisotropic surface diffusion of indium atoms on InP-based materials and the small lattice mismatch between InAs and InP lead to inhomogeneous size broadening of dots and formation of elongated dots [10, 11]. As a result, the energy levels, which are theoretically discrete, exhibit spectral broadening in practice, as evidenced by photoluminescence (PL) measurements [12]. Although precise control of growth parameters can improve the optical properties of QDs, variations in dot size remain inevitable, resulting in emission wavelength shifts beyond the target range and broader linewidths that degrade the device performance [13]. To address these challenges, two commonly adopted approaches are the indium-flush (IF) technique for self-assembled QDs [14–16] and the alternative growth (AG) method [17–19].

The IF technique involves the deposition of a first capping layer (FCL), such as a few nanometres of InAlGaAs, to partially cap the self-assembled QDs. This step results in the exposure of larger QDs that protrude above the FCL, owing to energetically unfavourable nucleation on the apex of the QDs. A subsequent thermal annealing step under arsenic pressure is then employed to selectively desorb indium from the uncapped regions of the QDs. This process effectively tailors the dot height, resulting in improved vertical size uniformity and a narrower full width at half maximum (FWHM) in PL. Moreover, the emission wavelength can be tuned by adjusting the FCL thickness.

The AG method differs from conventional self-assembled growth mode, where InAs is deposited continuously above the critical thickness to form the three-dimensional (3D) islands. In contrast, AG QDs are formed through a cyclic deposition process involving sub-or-quasi-critical thickness layers of InAs alternated with thin quantum well (QW) layers (e.g. InAlGaAs). The strain fields generated by lattice mismatch and intrinsic phase separation in each period influence the subsequent nucleation of vertically correlated In-rich clusters, thereby modulating QD formation in the following layers [17, 19–21]. By adjusting the InAs deposition thickness in each cycle, the QD size can be controlled, enabling tunability of the emission wavelength. This method is also expected to produce

QDs with narrower PL FWHM as vertical size fluctuations are effectively suppressed [20].

While both the IF and AG techniques have demonstrated efficacy in achieving wavelength tunability and emission linewidth narrowing in single-layer InAs/InP QDs, a direct and systematic comparison of their performance in multistacked configurations has not yet been reported. Given the critical importance of stacking multiple QD layers for enhancing optical gain in practical devices [22], this study uniquely investigates and contrasts the structural and optical evolution of five-stacked IF and AG nanostructures. Our work offers new insights into the stacking behaviour, morphology, and emission characteristics arising from these two distinct growth strategies.

In this work, we investigated the impact of IF and AG on single-layer and five-stacked configurations. To evaluate their structural and optical characteristics, we performed scanning transmission electron microscopy (STEM), atomic force microscopy (AFM), room-temperature PL measurements, and temperature-dependent PL measurements.

# 2. Methodology

All the InAs/InP QD samples were grown by a solidsource Veeco GEN-930 molecular beam epitaxy (MBE) system equipped with a valved arsenic cracker source on InP (001) substrates. The InP (001) substrates were degassed in the buffer chamber at 400 °C for an hour and then transferred to the growth chamber for a 1-minute deoxidation at 500 °C under As<sub>2</sub> overpressure. All the  $In_{0.524}Al_{0.476}As$  and In<sub>0.528</sub>Al<sub>0.238</sub>Ga<sub>0.234</sub>As layers employed are lattice-matched to InP. The schematic diagrams of the samples are illustrated in figure 1. For the IF samples as shown in figure 1(a), 500 nm InAlAs and 100 nm InAlGaAs buffer layers were deposited first at 510 °C and 500 °C, respectively. Then, 5.5 monolayers (MLs) of InAs QDs were grown at 485 °C using the S-K growth mode. A 4 nm FCL was then deposited to partially cap the QDs. Subsequently, the temperature was raised to 540 °C to flush the exposed portions of the QDs. For the single-layer IF QDs (IF1), a 96 nm InAlGaAs second capping layer (SCL) was applied at 500 °C. For the five-stacked IF QDs (IF5), a stacking structure was employed using a 26 nm SCL between subsequent QD layers, resulting in a total spacer thickness of 30 nm (4 nm FCL + 26 nm SCL) at 500 °C, followed by a final 70 nm InAlGaAs cap at 500 °C. For the AG samples as shown in figure 1(b), 200 nm InAlAs and 100 nm InAlGaAs buffer layers were first grown at 510 °C and 495 °C, respectively. Subsequently, 12 periods of 1 Ml InAs/1 Ml InAlGaAs were deposited at 485 °C to form the AG QDs. For the single-layer AG layer (AG1), a 100 nm InAlGaAs capping layer was applied. For the five-stacked AG layers (AG5), the stacking structure comprised AG structure separated by 30 nm

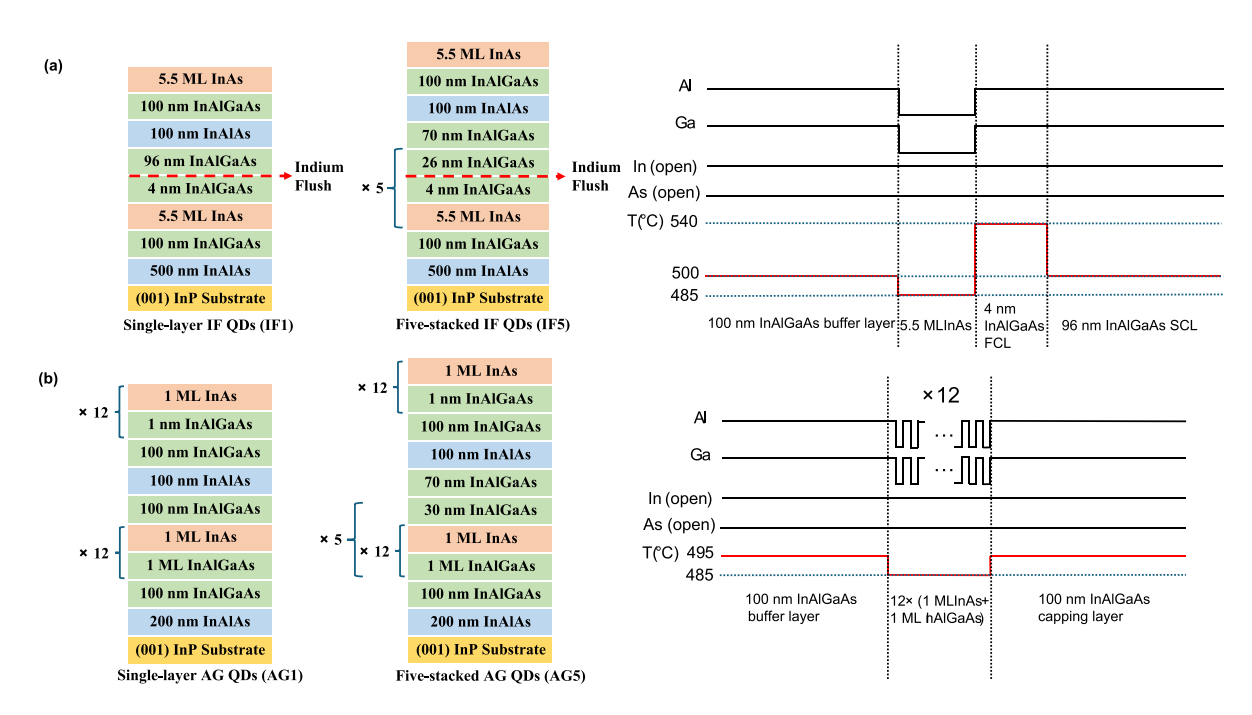


**Figure 1.** Schematic diagrams of InAs/InP QD structures grown with different techniques. (a) IF QDs: the single-layer structure (IF1) is shown on the left, the five-stacked structure (IF5) in the middle, and the schematic of the shutter opening sequence and temperature variation during MBE growth of the IF1 active region on the right. (b) AG samples: the single-layer structure (AG1) is shown on the left, the five-stacked structure (AG5) in the middle, and the schematic of the shutter opening sequence and temperature variation during MBE growth of the AG1 active region on the right. In the shutter opening sequence, a solid black line at the top indicates the shutter is open, while a solid black line at the bottom indicates the shutter is closed.

InAlGaAs spacers, followed by a final 70 nm InAlGaAs cap. All samples were additionally capped with a 100 nm InAlAs layer and a 100 nm InAlGaAs layer, followed by an uncapped active region layer grown under the same conditions as the underlying active region for AFM measurements.

STEM was performed to investigate the cross-sectional structural characteristics of the IF and AG samples. IF lamella was prepared using a standard FIB sample preparation in a Hitachi Ethos NX5000 with a final Ga<sup>+</sup> thinning at 5 keV. STEM analysis were carried out in a probe corrected cold-field emission gun Nion UltraSTEM100 at 100 keV with a convergence semi-angle of 30 mrad and a beam current of approximately 30 pA, yielding a probe size of 85 pm. AG lamellae were prepared with a Thermo Fisher Scientific Helios 5 Hydra UX PFIB with a 5 keV Xe<sup>+</sup> finishing, and STEM analyses were carried out using a probe corrected Thermo Fisher Scientific XFEG Spectra Ultra operated at 300 keV with a convergence semi-angle of 30 mrad and a beam current of approximately 60 pA, yielding probe sizes below 85 pm. In addition, AFM was employed to examine the surface morphology of the four samples, enabling direct comparison before and after stacking. PL measurements at room temperature were conducted using a Nanometrics RPM2000 system, incorporating a 635 nm continuous-wave laser at an excitation power density of 430 W cm<sup>-2</sup> and a wavelength-extended InGaAs detector with a cutoff at 2  $\mu$ m. The PL measurements were used to assess changes in emission wavelength and FWHM resulting from stacking. These characterisations provide valuable insights into the mechanisms by which IF and AG growth methods achieve wavelength tuning and linewidth narrowing, while also revealing the impact of stacking on the resulting structural and optical properties.

# 3. Results and discussion

#### 3.1. Scanning transmission electron microscopy

To investigate the cross-sectional morphology and interface quality of the samples, STEM high-angle annular dark-field (HAADF) imaging was employed.

A representative HAADF image acquired at 100 keV of IF QDs is displayed in figure 2(a). QDs that exceed the thickness of the FCL are truncated during the IF process, whereas shorter QDs remain unchanged. A curvature-like Al-rich region forms between adjacent QDs, identified by its darker contrast in the atomic-number () dependence of HAADF images, while In-rich regions with brighter contrast appear above the QDs. The underlying mechanism can be explained as follows. Upon reaching a critical thickness of the in-plane InAs wetting layer, 3D InAs islands are self-assembled due to the accumulation of strain arising from lattice mismatch. An FCL with a thickness lower than the height of most QDs is then deposited. Due to the elastic relaxation at the apex of QDs, which is an energetically unfavourable site for Ga and Al atoms, the growth of InAlGaAs is impeded atop the QDs. Consequently, this leads to a curvature in the capping layer at the edges where it contacts the QDs. Once the temperature is elevated under As<sub>2</sub> overpressure, the In atoms from both the exposed apexes of

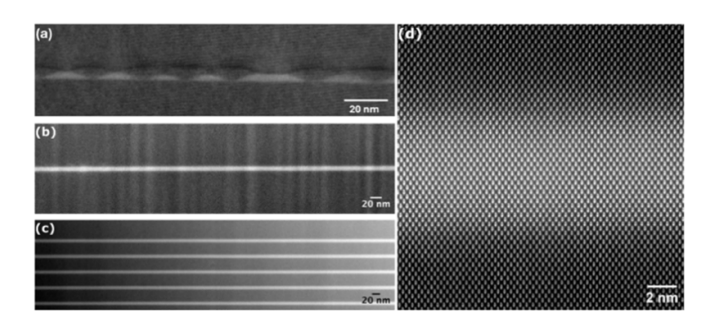


**Figure 2.** HAADF images showing the morphologies and adjacent layers of samples (a) IF1, (b) AG1, and (c) AG5. HAADF images of IF and AG samples were taken at 100 keV and 300 keV, respectively. (d) Atomic resolution HAADF image of the AG1, showing a well-like morphology.

QDs and the upper part within the capping layer desorb to the region above the capping layer. Initially, the In atoms migrate across the FCL, with the intention of establishing a new wetting layer [16]. However, the elevated temperature weakens the potential covalent bonds, leading to the detachment of the desorbed In atoms [23]. Throughout this process, the composition within the upper region of the FCL shifts towards an Alrich configuration due to the desorption of In atoms. This Alrich part acts as a protective layer for hindering further In evaporation. Meanwhile, the desorption of indium atoms within the QDs ceases once their height aligns with that of the adjacent InAlGaAs. As a result, the uncapped pyramid-like QDs transform into a disk-like shape after IF is applied. Next, the SCL is deposited to fully cap all the underlying structure. The top of the InAs QDs contains energetically favourable sites for following In adatoms, leading to the formation of In-rich region in the SCL. On the contrary, the upcoming Al atoms prefer to combine with the sites in the Al-rich region of FCL. In the stacked structure, the presence of In-rich and Al-rich regions within the spacer layer leads to apparent phase separation. However, this does not extend through the entire spacer to affect the subsequent QD layer [14]. In addition, the compressive strain at the top of the QDs is alleviated by the transformation from a pyramid-like to a truncated shape [14].

The images in figures 2(b)–(d) present the HAADF images of AG samples. Distinct QD-like nanostructures are not observed. Instead, the morphology more closely resembles QWs. For the five-stacked AG QD structures reported by Kim et al [20], prominent indium clusters appeared in the first layer. They claimed the AG QDs in the initial layer modified the strain field and phase separation properties of InAlGaAs, and the accumulated strain promoted QD formation in the subsequent layers. In our work, although the PL characteristics mentioned in later section are comparable to those reported by Kim et al in terms of emission wavelength and linewidth, we do not observe the formation of well-defined or high-density QD nanostructures. This suggests that the AG growth method may be inherently unstable (i.e. highly dependent on the initial

nucleation process) and does not consistently produce QDs. Although similar cyclic deposition techniques are widely used for growing submonolayer (SML) QDs on GaAs substrates [24-26], they may not be directly applicable to InP-based systems due to differences in lattice mismatch. In the case of GaAs substrates, the lattice mismatch with InAs is relatively large, resulting in stronger elastic strain during initial stages of growth. This enhanced strain promotes indium segregation and formation of QDs. For example, Kim et al reported InAs/InGaAs SML QDs [27] grown on GaAs, where their STEM micrographs revealed interfacial features similar to those observed in our AG samples, but with clearly visible indium clusters or agglomerations. In contrast, the use of InP substrates in our work leads to significantly lower strain, which makes the nucleation of well-defined QD-like features less favourable. In addition to the substrate effect, the material composition of the spacer layer also plays a critical role. The SML QD and AG QD formation mechanisms rely on indium atoms segregating during periodic deposition to form clusters or promote QD formation in the following layers. On GaAs substrates, this condition is easily met when spacers such as GaAs is used. However, in InP-based systems where both InAs and the quaternary spacer layer (e.g. InAlGaAs) contain indium. This suppresses effective indium segregation and thus inhibits the formation of distinct QD morphologies. Previous studies have also shown that SML QDs grown with indium-containing spacers tend to exhibit more QW-like morphology compared to other InAs/GaAs SML structures [27, 28]. This further supports the conclusion that indium in the spacer regions hinders the clustering process during alternating growth [18, 29, 30]. The STEM images in figures 2(b)-(d) also show that AG samples exhibit sharp and well-defined interfaces without apparent dislocations. This superior interface quality can be attributed to two factors. First, the AG scheme resembles that of a strain layer superlattice [31], where the strain introduced in each period is partially compensated during growth, leading to reduced overall strain accumulation. Second, the use of only 1 ML of InAs per period leads to reduced interface roughness and suppresses lateral In/Ga intermixing [32, 33]. As a result, the stacked AG5 sample exhibits high apparent crystal quality, as evidenced by sharp interfaces and a uniform composition throughout the entire structure, with no observable dislocations or structural degradation. Thus, the morphologies more closely resemble that of QWs rather than QDs. This indicates that the AG growth mode, when applied on an InP substrate, is significantly limited in its ability to form QDs. The insufficient elastic strain resulting from the relatively small lattice mismatch between InAs and InP, combined with the presence of indium in the spacer layer, likely inhibits effective indium segregation and thus suppresses the formation of well-defined QDts.

In comparison, IF and AG exhibit fundamentally different growth behaviours and resulting morphologies. IF enables well-defined, truncated QDs with clear size control and moderate strain management across stacked layers. In contrast,

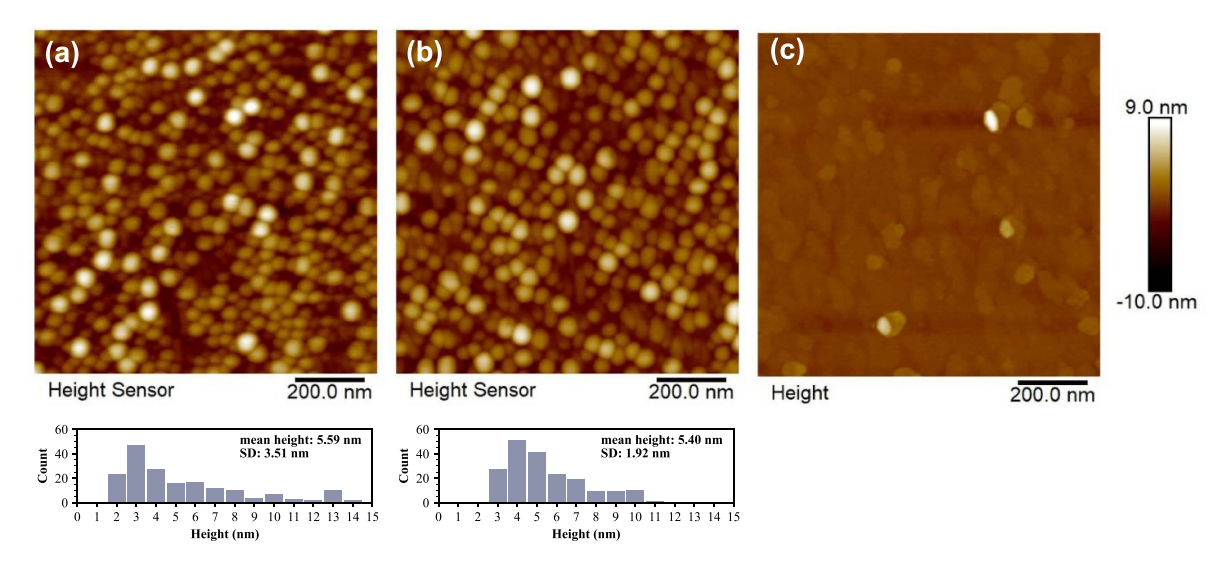


Figure 3. QD morphology in  $1 \times 1~\mu\text{m}^2$  AFM images of (a) IF1 [14], (b) fifth layer of IF5, and (c) AG1. In (a) and (b), the histogram below each AFM image shows the distribution of QD heights. For IF1, the average height is 5.59 nm with an SD of 3.51 nm. For IF5, the average height is 5.40 nm with an SD of 1.92 nm.

AG produces QW-like structures with sharp interfaces but lacks consistent dot formation, likely due to insufficient strain accumulation and suppressed indium segregation on InP substrates. While AG shows excellent crystalline quality, it does not reliably produce discrete QD features in the stacking configuration.

#### 3.2. Atomic force microscopy

While the STEM results provide insight into the crosssectional structural properties of the samples, AFM was employed to investigate the surface morphology associated with different growth approaches and stacking configurations.

Figure 3(a) corresponds to uncapped QDs without indium flush, directly exposed at the surface, confirming that the nanostructures in the first layer are primarily round-shaped dots. For the five-stacked IF QD sample as shown in figure 3(b), the growth was terminated immediately after the deposition of the fifth QD layer without applying a capping layer. Figure 3(b) reveals the presence of several elongated nanostructures resembling quantum dashes at the fifth layer, which correlates with the spectral broadening observed in the PL measurements of the five-stacked IF QDs, as discussed in the next section. This indicates that further optimisation of the multilayer morphology may be possible by optimising spacer thickness, FCL thickness, or introducing strain compensation schemes [34, 35]. Nevertheless, the majority of the surface nanostructures remain round-shaped, similar to those observed in IF1. The histogram below each AFM shows the distribution of QD heights. Specifically, IF1 exhibits an average height of 5.59 nm with a standard deviation (SD) of 3.51 nm, while IF5 has an average height of 5.40 nm with an SD of 1.92 nm. This indicates that the indium flush process reliably maintains dot height uniformity across multiple layers. AFM results suggest that the indium flush process effectively suppresses stress accumulation during multilayer stacking, thereby stabilising the QD morphology and facilitating the formation of uniform and well-aligned QDs across multiple layers.

Figure 3(c) shows  $1 \times 1 \mu m^2$  AFM images of AG1. In the AG1 image, several large dots are observed on the surface, along with a noticeable density of two-dimensional (2D) islands. These large dots are attributed to ripening, which inevitably occurs during heteroepitaxial growth. Under thermodynamic equilibrium conditions [36], small indium agglomerations tend to coalesce into larger islands through this process. The large dots may reach the critical size for plastic relaxation, which can introduce V-shaped defects that propagate toward the surface and potentially degrade device performance [36, 37]. However, the density of large QDs is relatively low, and such features are not clearly observed in the corresponding STEM images. The coexistence of small 2D islands and a limited number of large dots suggests that while some degree of indium segregation does occur, the fraction of material forming distinct QDs is small. By combining the AFM and STEM observations, it is evident that the overall morphology of AG samples more closely resembles a QW structure, as discussed in the previous section. This highlights that AG growth, in contrast to conventional self-assembled QD methods, requires more carefully optimised growth parameters in order to reliably achieve QD formation.

The AFM results further highlight the contrast between the two methods. IF samples maintain a predominantly dot-like morphology even after stacking, with only partial transformation into elongated nanostructures. AG samples, however, show a mixture of large ripened QDs and 2D islands, with low dot density and high structural uniformity indicative of QW-like behaviour. These differences reinforce the idea that IF offers better morphological control in multilayer structures, while AG requires further tuning to consistently induce dot nucleation.

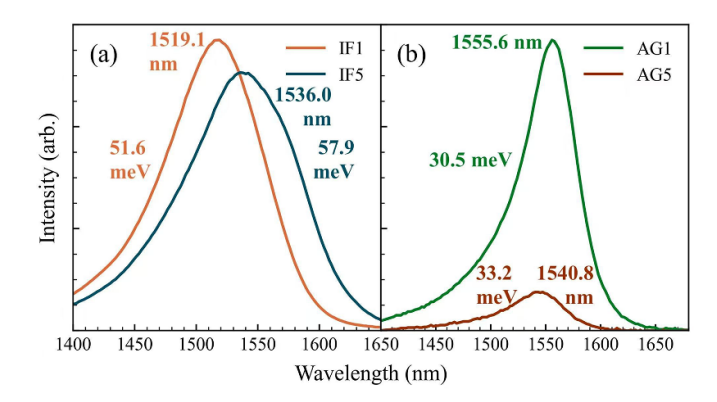


**Figure 4.** PL measurements for (a) IF QD samples and (b) AG QW samples.

#### 3.3. Room-temperature photoluminescence

To evaluate the optical impact of stacking on the QD structures with different growth techniques, room-temperature PL measurements were performed to compare the emission characteristics of single-layer and five-stacked QD samples.

For the IF samples, the PL peak wavelength redshifts from 1519.1 nm in IF1 to 1536.0 nm in IF5, accompanied by an broadening in FWHM from 51.6 meV to 57.9 meV, as shown in figure 4(a). The observed redshift is attributed to the inevitable increase in the average QD size in the upper stacking layers when the spacer layer is relatively thin, resulting from enhanced strain coupling during multilayer growth [38, 39]. However, the relatively small magnitude of this shift further confirms that the indium flush process effectively suppresses the majority of vertical strain build-up by producing heightuniform QDs, even in stacked configurations. The increase in FWHM arises not only from strain-induced size variation but also from the presence of additional elongated nanostructures, or quantum dashes, in the upper layers of IF5, as evidenced by AFM. This issue can be addressed through optimising spacer layer, FCL thickness, or by introducing strain compensation schemes as discussed in the previous section. The decrease in PL intensity is likely attributed to point defects formed during the deposition of the spacer layers. These defects act as non-radiative recombination centres, and their density increases with the number of stacked layers, thereby degrading emission efficiency. This issue may be mitigated by applying rapid thermal annealing (RTA) to suppress defectinduced non-radiative losses [40, 41].

For the AG samples, the PL peak exhibits a blueshift from 1555.6 nm in AG1 to 1547.6 nm in AG5, while the FWHM narrows from 30.5 meV to 29.7 meV, as shown in figure 4(b). The blue-shift in wavelength for multiple-stacked sample may be attributed to increased tensile strain in the stacked configuration [28, 42]. The nearly unchanged FWHM indicates that the surface of each AG layer remains relatively flat, with no significant additional strain introduced during stacking. This behaviour is more characteristic of QWs rather

than QDs. A noticeable reduction in PL intensity is observed in AG5, which is also due to the formation of point defects during the prolonged AG process. The previously mentioned post-growth RTA process can potentially be used to improve the crystal quality and optical characteristics for AG grown materials.

The PL results clearly reflect the morphological distinctions between IF and AG samples. The IF QDs exhibit a moderate redshift and linewidth broadening upon stacking, consistent with slight dot size variation and the occasional formation of quantum dashes. This behaviour aligns with that observed in conventional multi-stacked self-assembled QD structures reported in the literature [8, 38]. In contrast, the AG samples show minimal changes in FWHM and even a slight blueshift with stacking, indicating flat interfaces and low vertical strain—features more typical of QWs than QDs. Therefore, while AG yields narrow linewidths, IF offers greater potential for realising true QD-based emission in stacked configurations.

#### 3.4. Temperature-dependent photoluminescence

To further evaluate carrier confinement and thermal stability of the nanostructures, temperature-dependent PL measurements were performed on IF1 and AG1, as shown in figure 5. With increasing temperature, all PL spectra exhibit a gradual redshift, which is attributed to thermal-induced bandgap shrinkage caused by lattice constant expansion and electron—phonon interactions [27].

Meanwhile, the PL intensity decreases monotonically as temperature rises. This reduction originates from the activation of non-radiative recombination channels and the thermal escape of carriers from the QDs into the barrier layers, where they recombine without contributing to PL [43]. The integrated PL intensity was fitted using the Arrhenius equation:

$$I(T) = \frac{I_0}{1 + C\exp\left(-\frac{E_A}{kT}\right)} \tag{1}$$

where I(T) is the PL intensity at temperature T,  $I_0$  is the integrated PL intensity of the QD at T = 0 K, C is the fitting constant, k is the Boltzmann constant, and  $E_A$  is the thermal activation energy (TAE).

For IF1, the fitting yields a TAE of approximately 165 meV, indicating strong carrier confinement within the QDs. This high TAE indicates an effective suppression of non-radiative escape channels and high localisation of carriers inside QDs [44].

In contrast, AG1 exhibits a significantly smaller TAE of only 22 meV, which indicates weak carrier confinement. As a result, carriers in AG1 are more easily thermally delocalised, consistent with the quasi-QW-like morphology observed in STEM and AFM [45]. This behaviour is also evident in figure 5(b), where the PL intensity decreases by nearly half as the temperature increases from 80 K to 100 K. This reduced

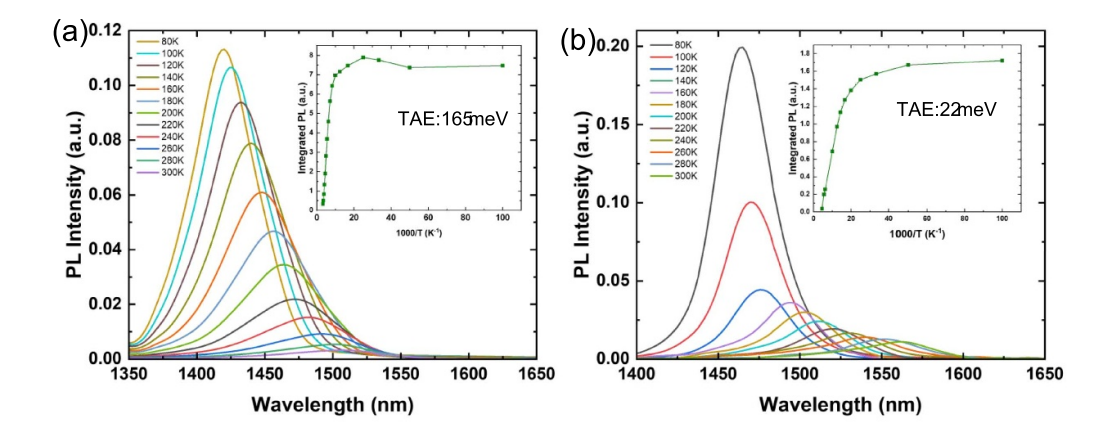


**Figure 5.** Temperature-dependent PL spectra of (a) IF1 and (b) AG1. The insets show the temperature dependence of the integrated PL intensity, from which the TAE values were extracted.

confinement directly limits the applicability of AG structures for temperature-stable laser operation.

These results highlight a clear contrast between IF and AG growth modes: while IF produces QDs with strong localisation and superior thermal stability, AG structures resemble QWs with insufficient confinement. Consequently, the IF method provides a more reliable platform for C-band QD devices that require high-temperature operation.

#### 4. Conclusion

In this work, we investigated the characteristics of single-layer and five-stacked InAs/InP QDs grown by MBE using IF and AG techniques. Structural and optical changes induced by stacking were examined by STEM, AFM, and room-temperature PL measurements. IF structures maintain uniform morphology across stacked layers by effectively limiting vertical strain through height control. However, some linewidth broadening occurs due to the formation of quantum dashes. In contrast, AG samples exhibit sharp interfaces and uniform composition throughout the entire structure, but the overall morphology resembles QWs rather than QDs. This is likely due to insufficient elastic strain and suppressed indium segregation on InP substrates. As a result, the AG method requires further optimisation strategies to reliably produce QDs on InP platforms.

Overall, this study demonstrates that IF represents a more reliable growth approach for achieving narrow-PL-linewidth C-band QDs on InP substrates, while AG growth must be carefully tailored to overcome its material system limitations. These findings provide valuable insight into the stacking behaviour of InAs/InP QDs grown by different techniques and offer guidance for the optimisation of multilayer QD configurations in future device applications.

# Data availability statement

All data that support the findings of this study are included within the article (and any supplementary files).

# Acknowledgment

This work was supported by UK Engineering and Physical Sciences Research Council (EP/V029606/1, EP/V029681/1, EP/Z532848/1, EP/X015300/1, EP/X035123/1, EP/W021080/1, EP/T028475/1, EP/S024441/1, EP/P006973/1); European Union's Horizon 2020 program (101129904).

#### **ORCID iDs**

Hui Jia © 0000-0002-8325-3948 Calum Dear © 0000-0003-1356-705X Huiwen Deng © 0000-0003-2680-152X Khalil El Hajraoui © 0000-0002-7627-6981 Mingchu Tang © 0000-0001-6626-3389 Huiyun Liu © 0000-0002-7654-8553

# References

- [1] Klotzkin D J 2020 Introduction to Semiconductor Lasers for Optical Communications (Springer)
- [2] Wada O 2004 Femtosecond all-optical devices for ultrafast communication and signal processing New J. Phys. 6 183
- [3] Portalupi S L, Jetter M and Michler P 2019 InAs quantum dots grown on metamorphic buffers as non-classical light sources at telecom C-band: a review *Semicond. Sci. Technol.* 34 053001
- [4] Lu Z, Liu J R, Raymond S, Poole P J, Barrios P J and Poitras D 2008 312-fs pulse generation from a passive C-band InAs/InP quantum dot mode-locked laser *Opt. Express* 16 10835–40
- [5] Asada M, Miyamoto Y and Suematsu Y 1986 Gain and the threshold of three-dimensional quantum-box lasers *IEEE J. Quantum Electron.* 22 1915–21
- [6] Wu J, Chen S, Seeds A and Liu H 2015 Quantum dot optoelectronic devices: lasers, photodetectors and solar cells J. Phys. D: Appl. Phys. 48 363001
- [7] Berg T W, Bischoff S, Magnusdottir I and Mork J 2001 Ultrafast gain recovery and modulation limitations in self-assembled quantum-dot devices *IEEE Photonics Technol. Lett.* 13 541–3

- [8] Park J-S et al 2025 Low threshold InAs/InP quantum dot lasers Opt. Express 33 19158–65
- [9] Feng Q, Wei W, Zhang B, Wang H, Wang J, Cong H, Wang T and Zhang J 2019 O-band and C/L-band III–V quantum dot lasers monolithically grown on Ge and Si substrate Appl. Sci. 9 385
- [10] Khan M Z M, Ng T K and Ooi B S 2014 Self-assembled InAs/InP quantum dots and quantum dashes: material structures and devices *Prog. Quantum Electron.* 38 237–313
- [11] Stintz A, Rotter T and Malloy K 2003 Formation of quantum wires and quantum dots on buffer layers grown on InP substrates J. Cryst. Growth 255 266–72
- [12] Ghadi H, Sehara N, Murkute P and Chakrabarti S 2017 Minimization of material inter-diffusion for thermally stable quaternary-capped InAs quantum dot via strain modification Superlattices Microstruct. 105 117–31
- [13] Yu X, Jia H, Dear C, Yuan J, Deng H, Tang M and Liu H 2023 Optically enhanced single-and multi-stacked 1.55 μm InAs/InAlGaAs/InP quantum dots for laser applications J. Appl. Phys. 56 285101
- [14] Yuan J et al 2024 Indium-flush technique for C-band InAs/InP quantum dots APL Mater. 12 121109
- [15] Keizer J, Clark E, Bichler M, Abstreiter G, Finley J and Koenraad P 2010 An atomically resolved study of InGaAs quantum dot layers grown with an indium flushstep *Nanotechnology* 21 215705
- [16] Wasilewski Z, Fafard S and McCaffrey J 1999 Size and shape engineering of vertically stacked self-assembled quantum dots J. Cryst. Growth 201 1131–5
- [17] Kim J S, Lee J H, Hong S U, Kwack H-S, Choi B S and Oh D K 2005 Well-defined excited states of self-assembled InAs/InAlGaAs quantum dots on InP (001) Appl. Phys. Lett. 87 053102
- [18] Kim J S, Lee J H, Hong S U, Han W S, Kwack H-S, Kim J H and Oh D K 2003 Structural and optical properties of shape-engineered InAs quantum dots J. Appl. Phys. 94 2486–90
- [19] Kim J S, Lee C-R, Lee I H, Leem J-Y, Kim J S and Ryu M-Y 2007 Formation characteristics of shape-engineered InAs/InAlGaAs quantum dots grown on InP substrates J. Appl. Phys. 102 073501
- [20] Kim J S, Lee C-R, Choi B S, Kwack H-S, Lee C W, Sim E D and Oh D K 2007 Vertical stacks of shape-engineered InAs/InAlGaAs quantum dot and its influences on the lasing characteristics Appl. Phys. Lett. 90 153111
- [21] Lee H, Lee C-R, Ahn H-K, Kim J S and Ryu M-Y 2016 Emission characteristics of shape-engineered InAs/InAlGaAs quantum dots subjected to thermal treatments J. Korean Phys. Soc. 69 85–90
- [22] Ledentsov N et al 1996 Direct formation of vertically coupled quantum dots in Stranski-Krastanow growth Phys. Rev. B 54 8743
- [23] Radhakrishnan K, Yoon S, Gopalakrishnan R and Tan K 1994 Indium desorption from strained InGaAs/GaAs quantum wells grown by molecular beam epitaxy J. Vac. Sci. Technol. A 12 1124–8
- [24] Lam P, Wu J, Tang M, Jiang Q, Hatch S, Beanland R, Wilson J, Allison R and Liu H 2014 Submonolayer InGaAs/GaAs quantum dot solar cells Sol. Energy Mater. Sol. Cells 126 83–87
- [25] Leem J-Y, Jeon M, Lee J, Cho G, Lee C-R, Kim J S, Kang S-K, Ban S, Lee J and Cho H K 2003 Influence of GaAs/InAs quasi-monolayer on the structural and optical properties of InAs/GaAs quantum dots J. Cryst. Growth 252 493–8

- [26] Xu Z, Birkedal D, Hvam J M, Zhao Z, Liu Y, Yang K, Kanjilal A and Sadowski J 2003 Structure and optical anisotropy of vertically correlated submonolayer InAs/GaAs quantum dots Appl. Phys. Lett. 82 3859–61
- [27] Kim J S, Shin J C, Kim J O, Noh S K, Lee S J and Krishna S 2019 Photoluminescence study of InAs/InGaAs sub-monolayer quantum dot infrared photodetectors with various numbers of multiple stack layers *J. Lumin*. 207 512–9
- [28] Shriram S R, Kumar R, Panda D, Saha J, Tongbram B, Mantri M R, Gazi S A, Mandal A and Chakrabarti S 2020 Study on inter band and inter sub-band optical transitions with varying InAs/InGaAs sub-monolayer quantum dot heterostructure stacks grown by molecular beam epitaxy IEEE Trans. Nanotechnol. 19 601–8
- [29] Mukai K and Sugawara M 1999 Suppression of temperature sensitivity of interband emission energy in 1.3-\(\mu\)m-region by an InGaAs overgrowth on self-assembled InGaAs/GaAs quantum dots Appl. Phys. Lett. 74 3963-5
- [30] Nishi K, Saito H, Sugou S and Lee J-S 1999 A narrow photoluminescence linewidth of 21 meV at 1.35 μm from strain-reduced InAs quantum dots covered by In 0.2 Ga 0.8 As grown on GaAs substrates Appl. Phys. Lett. 74 1111–3
- [31] Osbourn G 1982 Strained-layer superlattices from lattice mismatched materials J. Appl. Phys. 53 1586–9
- [32] Alnami N, Kumar R, Kuchuk A, Maidaniuk Y, Saha S K, Alnami A A, Alhelais R, Kawagy A, Ware M E and Mazur Y I 2021 InAs nanostructures for solar cell: improved efficiency by submonolayer quantum dot Sol. Energy Mater. Sol. Cells 224 111026
- [33] Kumar R, Maidaniuk Y, Kuchuk A, Saha S K, Ghosh P K, Mazur Y I, Ware M E and Salamo G J 2018 Excitation intensity and thickness dependent emission mechanism from an ultrathin InAs layer in GaAs matrix J. Appl. Phys. 124 235303
- [34] Celibert V, Tranvouez E, Guillot G, Bru-Chevallier C, Grenouillet L, Duvaut P, Gilet P, Ballet P and Million A 2005 MBE growth optimization and optical spectroscopy of InAs/GaAs quantum dots emitting at 1.3 μm in single and stacked layers J. Cryst. Growth 275 e2313–19
- [35] Akahane K, Ohtani N, Okada Y and Kawabe M 2002 Fabrication of ultra-high density InAs-stacked quantum dots by strain-controlled growth on InP (3 1 1) B substrate J. Cryst. Growth 245 31–36
- [36] Frigeri P, Nasi L, Prezioso M, Seravalli L, Trevisi G, Gombia E, Mosca R, Germini F, Bocchi C and Franchi S 2007 Effects of the quantum dot ripening in high-coverage InAs/ GaAs nanostructures J. Appl. Phys. 102 083506
- [37] Seravalli L, Frigeri P, Nasi L, Trevisi G and Bocchi C 2010 Metamorphic quantum dots: quite different nanostructures J. Appl. Phys. 108 064324
- [38] Kim J S 2006 Self-assembled InAs quantum dots with two different matrix materials J. Cryst. Growth 290 384–7
- [39] Oh J W, Ryu M-Y, Jo B, Kim J S, Harris T and Yeo Y K 2013 Bimodal luminescence behavior of spatially-ordered seven-stacked InAs/InAlGaAs quantum dots *Thin Solid* Films 541 68–71
- [40] Dear C *et al* 2025 The effect of rapid thermal annealing on 1.55 μm InAs/InP quantum dots *J. Appl. Phys.* **58** 125104
- [41] Li W, Chen S, Tang M, Wu J, Hogg R, Seeds A, Liu H and Ross I 2018 Effect of rapid thermal annealing on threading dislocation density in III–V epilayers monolithically grown on silicon J. Appl. Phys. 123 215303

- [42] Shriram S R, Gazi S A, Kumar R, Saha J, Panda D, Mandal A and Chakrabarti S 2020 Study on optical properties and strain distribution of InAs/InGaAs sub-monolayer quantum dot heterostructure with multiple stacking layers *Proc. SPIE* 11345 294–301
- [43] Xu Z Y, Lu Z D, Yuan Z L, Yang X P, Zheng B Z, Xu J Z, Ge W K, Wang Y, Wang J and Chang L L 1998 Thermal activation and thermal transfer of localized excitons in InAs
- self-organized quantum dots  $Superlattices\ Microstruct.$  23 381-7
- [44] Jahan N A *et al* 2013 Temperature dependent carrier dynamics in telecommunication band InAs quantum dots and dashes grown on InP substrates *J. Appl. Phys.* **113** 033506
- [45] Torchynska T V 2008 Some aspects of exciton thermal exchange in InAs quantum dots coupled with InGaAs/GaAs quantum wells J. Appl. Phys. 104 074315